

THE CANADIAN MINERALOGIST

Canadian Mineralogist
Vol. 27, pp. 545-563 (1989)

SKARN FORMATION AT THE MACMILLAN PASS TUNGSTEN DEPOSIT (MACTUNG), YUKON AND NORTHWEST TERRITORIES. I. P-T-X-V CHARACTERIZATION OF THE METHANE-BEARING, SKARN-FORMING FLUIDS

MICHAEL R. GERSTNER¹ AND JOHN R. BOWMAN

Department of Geology and Geophysics, University of Utah, Salt Lake City, Utah 84112, U.S.A.

JILL D. PASTERIS

Department of Earth and Planetary Sciences, Washington University, Box 1169, St. Louis, Missouri 63130, U.S.A.

ABSTRACT

Microthermometric and Raman spectroscopic analyses of fluid inclusions from the MacTung scheelite skarn deposit indicate that the skarn-forming fluids are water-dominant, low in salinity, and methane-bearing. In general, the measured salinities are less than 5.0 equivalent wt. % NaCl. Calculated values of $X(\text{CH}_4)$ in the bulk fluid range from 0.005 to 0.02 in inclusions in pyroxene skarn, and from 0.01 to 0.04 in inclusions in garnet and quartz from both anhydrous and hydrous skarn. Carbon dioxide is a very minor component [$X(\text{CO}_2) \ll 0.01$] in the skarn fluid from all facies. The measured final homogenization temperatures and calculated pressures of the methane-bearing aqueous fluids indicate minimum trapping temperatures and pressures of 355°C and 2.1 kbar for inclusions in hydrous and garnet skarn, and 335°C and 1.4 kbars for inclusions in pyroxene skarn. On the assumption of a maximum fluid pressure of 2.5 kbars, many inclusions in the pyroxene, garnet, and amphibole skarns have essentially indistinguishable trapping temperatures near 380°C. The greater part of the pyroxene skarn formed at somewhat higher temperatures, from 410 to 470°C (430°C av.). The majority of inclusions in garnet and amphibole skarns have virtually identical calculated isochores. The similarities in trapping temperatures indicate significant overlap in pressure-temperature conditions for the formation of anhydrous and initial hydrous skarn. The biotite facies of hydrous skarn

began forming at similar *P-T* conditions, but continued to develop after pyroxene, garnet, and amphibole skarns ceased to form, as the temperature fell to 325°C. The fluid-inclusion data indicate that some variations in temperature and probably fluid pressure occurred within all skarn types. Fluid pressures closely approached lithostatic pressure (2.5 kbar maximum) throughout skarn development, but very likely fluctuated between probable limits of 2.1 to 2.5 kbars. Maximum decreases in temperature, calculated by assuming a constant fluid pressure, are less than 150°C from the earliest (highest *T*) pyroxene skarn to the latest (lowest *T*) biotite skarn. The most significant differences in temperature occur *within* anhydrous skarn development (*i.e.*, between pyroxene and garnet skarn) and *within* hydrous skarn development (*i.e.*, between amphibole and biotite skarn). The anhydrous garnet skarn and the hydrous amphibole skarn formed at virtually indistinguishable *P-T* conditions. Thus, there is no significant break in *P-T* conditions between the development of "prograde" anhydrous and "retrograde" hydrous skarn types at MacTung.

Keywords: skarn, fluid inclusions, tungsten, temperature, pressure, MacTung, Yukon Territories, Northwest Territories.

SOMMAIRE

Les analyses microthermométriques et par spectroscopie de Raman, effectuées sur des inclusions fluides prélevées du gisement de scheelite de MacTung, sur la frontière du Yukon et des Territoires du Nord-Ouest, montrent que

¹Present Address: Delta Environmental Consultants, Inc., Fort Collins, Colorado 80526, U.S.A.

la phase fluide qui a accompagné la formation du skarn était en grande partie de l'eau, à salinité et teneur en méthane faibles. En général, les salinités mesurées sont inférieures à 5.0% par poids en équivalents de NaCl. Les valeurs calculées de $X(\text{CH}_4)$ varient de 0.005 à 0.02 dans les inclusions provenant du skarn à pyroxène, et de 0.01 à 0.04 dans les inclusions piégées dans le grenat et le quartz des skarns anhydre et hydraté. Le CO_2 est un composant très peu important [$X(\text{CO}_2) < 0.01$] dans le fluide échantillonné dans tous les facies. Les températures d'homogénéisation finale des fluides contenant du méthane et les pressions dérivées indiquent une température et une pression minimales de piégeage de 355°C et 2.1 kbars pour les skarns hydraté et grenatifère, et 335°C et 1.4 kbars pour le skarn à pyroxène. En supposant que la pression n'a pas dépassé 2.5 kbars, plusieurs inclusions des skarns à pyroxène, grenat et amphibole révèlent une température de piégeage uniforme près de 380°C. En grande partie, le skarn à pyroxène se serait formé à une température plus élevée, entre 410 et 470°C (en moyenne, 430°C). En majorité, les inclusions des skarns à amphibole et à grenat contiennent des isochores calculés quasiment identiques. Les ressemblances des températures de piégeage montrent qu'il y a eu un chevauchement important des conditions de température et de pression lors de la formation des skarns anhydre et initialement hydraté. Le facies à biotite du skarn hydraté s'est d'abord formé à des conditions semblables, mais il a continué à se développer aux températures inférieures à 325°C, après que les skarns à pyroxène, grenat et amphibole eurent cessé d'évoluer. Les inclusions fluides indiquent quelques variations en température et, tout probablement, en pression de la phase fluide dans tous les facies. La pression de la phase fluide aurait presque atteint la pression lithostatique (maximum 2.5 kbars) à travers le système, tout en fluctuant entre 2.1 et cette limite. Le décalage maximal dans la température de formation, calculée en supposant une pression constante de la phase fluide, aurait été inférieur à 150°C entre les skarns à pyroxène (précoce, température élevée) et à biotite (tardif, température plus basse). Les variations les plus importantes se manifestent parmi les skarns anhydres (entre skarn à pyroxène et skarn à grenat) et parmi les skarns hydratés (entre skarn à amphibole et skarn à biotite). Le skarn anhydre à grenat et le skarn hydraté à amphibole se sont formés à des conditions de P et T quasiment identiques. Il n'y aurait donc pas eu d'interruption importante dans ces conditions lors du développement des skarns "progrades", qui sont anhydres, et rétrogrades, qui sont hydratés.

(Traduit par la Rédaction)

Mots-clés: skarn, inclusions fluides, tungstène, température, pression, MacTung, Yukon, Territoires du Nord-Ouest.

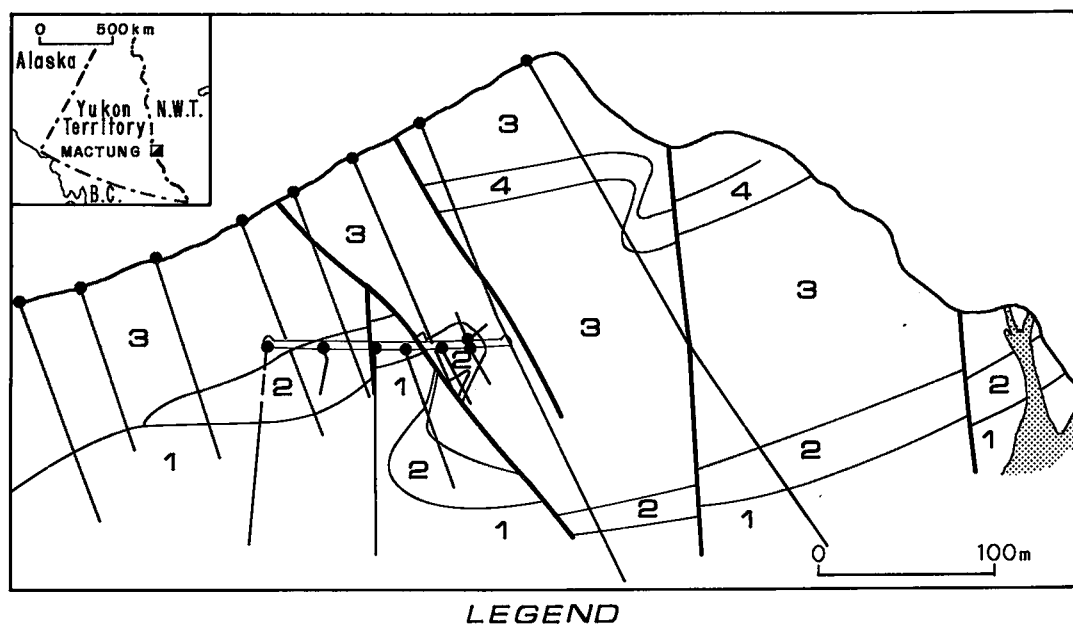
INTRODUCTION

Skarn deposits historically have been an important source of tungsten. The scheelite skarn deposit at MacTung, on the Northwest Territories-Yukon border, represents one of the major scheelite concentrations in the world. Despite several recent studies (Newberry 1982, Mathieson & Clark 1984,

Bowman *et al.* 1985, Brown *et al.* 1985), relatively little is known about tungsten skarns in terms of the detailed physicochemical conditions of their development, especially the time and space variations in pressure and temperature, the fugacities of gas species, and the activities of dissolved aqueous species responsible for their formation.

Pressure, temperature, and the proportions of the major gaseous species (including CO_2 , CH_4 , and H_2S) have been proposed as important variables in skarn petrogenesis in general (Burt 1971a, b, Einaudi *et al.* 1981) and for tungsten skarn deposits in particular (Dick & Hodgson 1982, Newberry 1982). Newberry (1982) and Einaudi *et al.* (1981) have proposed that in the case of tungsten skarns, the early, largely anhydrous skarn assemblages formed at high temperatures (> 500 to 650°C) and that the later retrograde hydrous skarn assemblages formed at distinctly lower temperatures, and from different fluids. Using a quantitative approach based on phase equilibria and stable isotopes, Brown *et al.* (1985) demonstrated that in the Pine Creek (California) skarns, early anhydrous skarn developed at high temperatures ($\leq 560^\circ\text{C}$), and later hydrous skarn developed in response to a significant influx of meteoric water. In contrast, Dick & Hodgson (1982) interpreted the suite of hydrous and anhydrous mineral assemblages characteristic of skarns in the northern Cordillera as a result of essentially simultaneous formation at similar pressures and temperatures in response to variations in chemical variables. In a fluid-inclusion study of the CanTung scheelite skarn deposit, located almost 200 km south of the MacTung deposit, Mathieson & Clark (1984) proposed that although a temperature decrease occurred from early anhydrous skarn to later, hydrous skarn formation, much of the anhydrous skarn formed at temperatures and pressures similar to those of the hydrous skarn. Mathieson & Clark (1984) found that CO_2 and CH_4 were present in many of the fluid inclusions from CanTung but did not characterize the $X(\text{CO}_2)/X(\text{CH}_4)$ ratio or test for the presence of other gaseous species.

Several studies (Cook 1982, Meinert & Hawksworth 1983, Mathieson & Clark 1984, Kemp 1985, Turner 1985, Connelly & Bowman 1990) have demonstrated that reliable data on P , T , and fluid compositions in skarn systems can be gained from fluid-inclusion microthermometry. The combined application of Raman spectroscopy and microthermometry to fluid-inclusion analysis in deposits from other geological environments has been shown (*e.g.*, Ramboz *et al.* 1985, Pasteris *et al.* 1986) to yield more accurate determinations of fluid compositions than the use of either technique alone, especially with regard to the proportions of the major gaseous species. This combination, therefore, provides better estimates of pressures and temperatures than can



LEGEND

- | | | | |
|---|---------------------------|---|---------------------------|
| ① | PHYLLITE | ③ | HORNFELS |
| ② | LOWER CARBONATE,
SKARN | ④ | UPPER CARBONATE,
SKARN |
| ▨ | QUARTZ MONZONITE | — | DRILL HOLE |

FIG. 1. North-south cross-section (section 21811E) through the MacTung deposit (after AMAX geological staff), looking west. This section was studied in detail by Dick (1976) and Dick & Hodgson (1982). Diamond drill holes and a cross-cut of the underground exploratory adit intersected by the cross-section also are shown.

normally be achieved by using microthermometry alone.

This paper is the first of a series of three dealing with the origin of the MacTung tungsten (copper) skarns. It concerns the results of a fluid-inclusion study that addressed the following goals: (1) determination of the pressure-temperature conditions and fluid composition during all stages of skarn formation, and (2) development of a framework for subsequent analysis of other variables that are potentially important in skarn formation, including $f(\text{O}_2)$, $f(\text{S}_2)$, activities of aqueous ionic species, and the sources of C, S, and H_2O in the skarn. Part II will develop the detailed physicochemical environment of skarn formation. Part III will present the results of stable-isotope studies focused on the origin and isotopic evolution of the skarn fluids.

GENERAL GEOLOGY

The MacTung tungsten (copper) deposit, one of several important skarn deposits in the northwestern Canadian cordillera, is located on the Yukon-

Northwest Territories border, in the Selwyn Mountain range ($63^\circ 17' \text{N}$, $130^\circ 30' \text{W}$). The general geology of the deposit has been described by Dick (1976), Harris (1977), and Dick & Hodgson (1982), and will only be summarized here. As shown in the cross section (Fig. 1), the deposit is located in two main Lower Paleozoic carbonate units, now largely replaced by

TABLE 1. SKARN MINERAL ASSEMBLAGES IN THE MACTUNG DEPOSIT*

Anhydrous skarn	
I.	Pyroxene skarn pyroxene, quartz, scheelite, pyrrhotite, ± titanite ± wollastonite
II.	Garnet skarn garnet, quartz, pyrrhotite ± scheelite ± calcite ± titanite ± chalcopyrite
Hydrous skarn	
III.	Amphibole skarn amphibole, quartz, pyrrhotite ± clinozoisite ± calcite ± scheelite ± plagioclase ± apatite ± titanite
IV.	Biotite skarn biotite, quartz, pyrrhotite ± apatite ± plagioclase ± chlorite

* after Dick & Hodgson (1982) and Gerstner (1987)

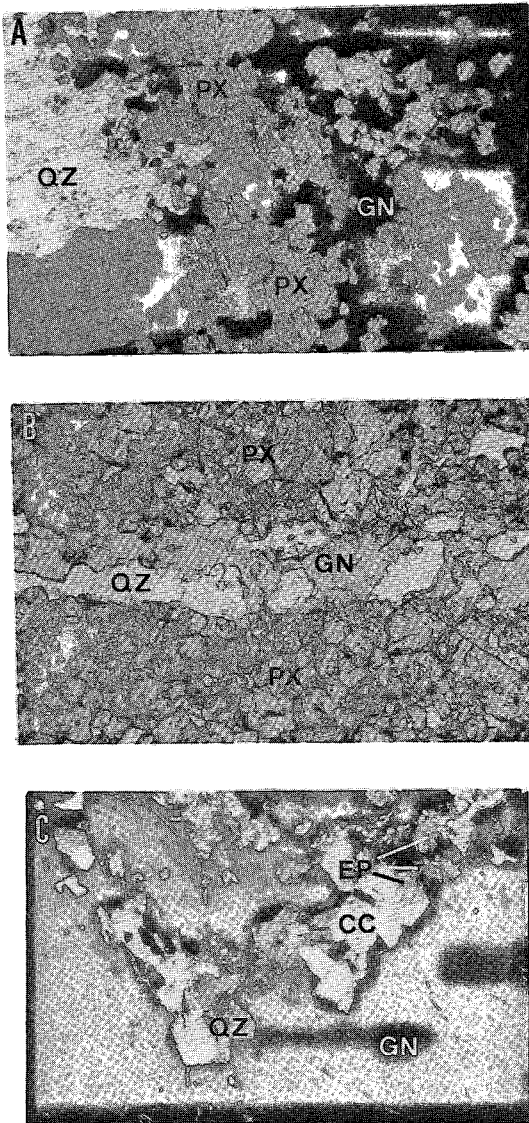


FIG. 2. A. Photomicrograph showing hedenbergitic pyroxene (PX) replaced by garnet (GN) and quartz (QZ). The two segments of pyroxene in the center of the photograph are optically continuous and are now separated as a result of the partial replacement by garnet and quartz. Crossed nicols. $\times 2.5$. B. Photomicrograph showing massive pyroxene (PX) skarn cross-cut by a vein of garnet (GN) + quartz (QZ) (garnet skarn) Plane light. $\times 2.5$. C. Photomicrograph showing garnet (GN) partly replaced at its margin by epidote (EP), quartz (QZ), and calcite (CC). Crossed nicols. $\times 2.5$.

skarn, which are interbedded with hornfels; these units overlie a micaceous phyllite. An Upper Cretaceous monzogranite crops out north of the deposit.

The skarn mineralogy and paragenesis of the deposit have been described by Dick (1976) and Dick & Hodgson (1982), and are summarized in Table 1; further details are included in Part II of this study and in Gerstner (1987). Within the two major subdivisions of anhydrous and hydrous skarn at MacTung, there are four distinct assemblages of skarn minerals. Pyroxene-rich skarn (I in Table 1) is volumetrically the most important rock-type in the deposit. Within the anhydrous skarn, pyroxene is commonly replaced by quartz, garnet and pyrrhotite (Fig. 2A), which are the characteristic minerals of assemblage II. In thin section, large grains of garnet typically mantle smaller grains of pyroxene. Also, quartz-garnet veins cross-cut pyroxene skarn (Fig. 2B). However, mantling and replacement of garnet by pyroxene, reported by Dick (1976), were not observed.

Texturally, hydrous skarn is massive, overprints anhydrous skarn, and occurs as veins that cross-cut anhydrous skarn. The replacement of pyroxene by amphibole, quartz, calcite and pyrrhotite, or of garnet by clinozoisite, quartz and calcite (Fig. 2C), mineralogically characterizes the development of hydrous skarn. Amphibole- and clinozoisite-bearing assemblages (III in Table 1) comprise the majority of the hydrous skarn. Biotite, which occurs more rarely, replaces amphibole in massive hydrous skarn and forms selvages around quartz veins that cross-cut amphibole skarn. Biotite skarn (IV in Table 1) was not observed in direct contact with anhydrous skarn or as a direct replacement of anhydrous skarn. Nor was hydrous skarn observed to replace marble, as it does in the CanTung skarn (Mathieson & Clark 1984).

At any location within the MacTung deposit, detailed textural relationships in thin section and hand specimen indicate the following temporal sequence of skarn development: 1) pyroxene skarn; 2) garnet-quartz skarn; 3) amphibole-clinozoisite-calcite skarn; and 4) biotite skarn. Such small-scale textural relationships do not establish the absolute timing for formation of individual facies within the entire deposit, but only the sequence of replacement at any single location. Both Mathieson & Clark (1984) and Bowman *et al.* (1985) have emphasized that different skarn facies could form at the same time at different locations within a deposit; subsequent migration of boundaries between skarn facies could then generate the small-scale replacement relationships observed.

The pelitic hornfels adjacent to the skarn also is zoned (Dick & Hodgson 1982). Proceeding toward either skarn or cross-cutting quartz veins, the unaltered, graphitic, black hornfels has been progressively altered to light brown hornfels, dark brown hornfels, and light green hornfels. The minerals present in each hornfels zone are listed in Table 2.

The light green hornfels consists of calc-silicate mineral assemblages and is itself zoned. The appearance of amphibole and titanite marks the beginning of the light green hornfels, and is followed toward the skarn and the cross-cutting quartz veins by pyroxene and quartz, which make up the largest volume of the light green hornfels. Light green hornfels is not always developed; where it is absent, dark brown hornfels occurs adjacent to skarn. Black graphitic hornfels is nowhere in direct contact with skarn, light green hornfels, or cross-cutting quartz veins. The mineralogical transitions from biotite to amphibole to pyroxene hornfels mirror the development of the different mineral assemblages in the skarn. This zonation led Dick (1976) and Dick & Hodgson (1982) to propose that the light green hornfels and skarn, including their respective facies, formed essentially simultaneously, and at similar temperatures and pressures. They inferred that the mineralogical zonation in both the hornfels and skarn reflect variations in the activities of aqueous ionic species; however, they did not have P - T data to test their hypothesis.

ANALYSIS OF FLUID INCLUSIONS

Fluid inclusions: types and procedures

In anhydrous skarn, fluid inclusions suitable for analysis were found in pyroxene, garnet and quartz, whereas in hydrous skarn, suitable fluid inclusions occur primarily in quartz and rarely in apatite and amphibole. Within these minerals single, equant and isolated fluid inclusions are distributed randomly within individual grains and are interpreted to be primary inclusions (Table 2-1, Roedder 1984). Trains of smaller inclusions are aligned along microfractures, particularly in quartz, and are interpreted as secondary inclusions. These latter inclusions are water-rich, occasionally with a carbonic (CO_2 - CH_4) fluid phase (see below; Gerstner 1987). Analyses reported here are for the fluid inclusions identified as being primary. At room temperature, almost all the primary inclusions are two-phase, consisting of an aqueous liquid and a central, lower-density, CH_4 -rich supercritical fluid (Figs. 3A-H). The inclusions are aqueous-phase-dominant, with a volume proportion of the aqueous liquid (f_a) between 0.85 and 0.65 at room temperature. Values of f_a are relatively constant in each sample, and no evidence exists for entrapment of boiling fluids. Three-phase inclusions are present in apatite crystals in sample MT68-003-6 (CO_2 liquid and vapor and aqueous liquid) and in quartz in sample MT-D-2 (CH_4 vapor, aqueous liquid, and hexagonal, opaque daughter crystals) (Fig. 3H).

Polished chips were made from 14 samples of anhydrous skarn and 15 samples of hydrous skarn. Based on a detailed petrographic inspection of over

TABLE 2. HORNFELS MINERALOGY, MACTUNG DEPOSIT*

Unaltered Hornfels	quartz, muscovite, biotite, graphite, pyrite, K-feldspar, rutile
Light Brown Hornfels	quartz, muscovite, biotite, pyrite, K-feldspar, rutile
Dark Brown Hornfels	quartz, biotite, pyrite ± muscovite ± titanite ± rutile ± K-feldspar
Light Green Hornfels	a) amphibole, quartz, titanite ± plagioclase b) pyroxene, quartz, titanite ± plagioclase

*after Dick (1976) and Dick & Hodgson (1982)

200 documented core and surface samples and accompanying thin sections, the samples selected for analysis are representative of the skarn and clearly show the textural and paragenetic relationships among skarn types. Geological descriptions, mineral assemblages and paragenesis are discussed in Gerstner (1987) and summarized in Table 1. Additional information on sample locations and descriptions is available from the Depository of Unpublished Data, CISTI, National Research Council of Canada, Ottawa, Ontario K1A 0S2 (Appendix A). Microthermometric measurements were performed on Chaixmecca and Fluid Inc. stages. All measurements reported here, with the exception of the partial homogenization temperatures (T_{ph}), were repeated at least twice; those inclusions in which the clathrate melting (T_{cm}), final ice melting (T_{im}), and total homogenization (T_{th}) temperatures could not be replicated to within $\pm 0.2^\circ$, $\pm 0.2^\circ\text{C}$, and 2°C , respectively, were discarded. Temperature measurements are considered accurate to $\pm 0.1^\circ\text{C}$ in the range -20° to $+20^\circ\text{C}$, and $\pm 1^\circ\text{C}$ below -60°C and over 300°C , based on repetitive measurements of laboratory melting standards and NaCl-water solutions of known composition. Laser Raman microprobe (LRM) analyses were done on the nonaqueous portion of 35 fluid inclusions from one sample of anhydrous skarn and four samples of hydrous skarn. The instrument used in this study is a 1983 model RAMANOR U-1000 microprobe, as described in Pasteris *et al.* (1986) and Wopenka & Pasteris (1986). The 514.5 nm line of a 5-watt Ar^+ laser was used for the analyses. The power was about 10 mW at the sample surface. An 80 \times microscope objective with a numerical aperture of 0.90 was used both to focus the laser into the sample and to collect the Raman-scattered radiation. The following spectral ranges were scanned: 1370-1400 cm^{-1} (CO_2); 2130-2160 cm^{-1} (CO); 2310-2350 cm^{-1} (N_2); 2580-2630 cm^{-1} (H_2S); 2900-2930 cm^{-1} (CH_4); 570-600 and 4120-4180 cm^{-1} (H_2); and 2860-2960

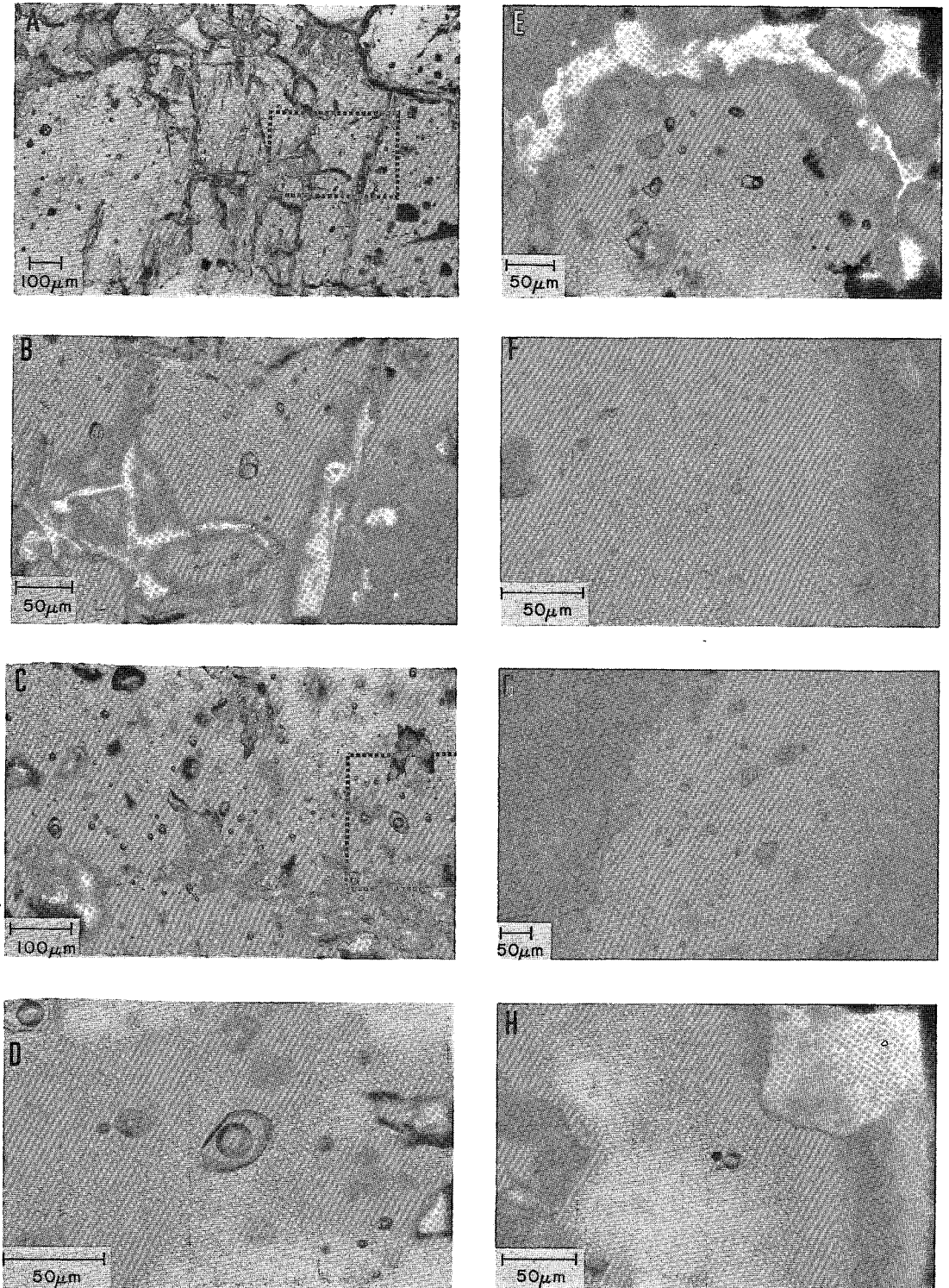


FIG. 3. Photomicrographs of fluid inclusions in thin, doubly polished plates (in plane-polarized transmitted light).

cm^{-1} (higher hydrocarbons). Measurements were made at 0.5 cm^{-1} stepping intervals in these frequency ranges, with 10-s counting times per step.

Low-temperature partial homogenization

On cooling, the inclusions exhibit "double freezing", with initial clathrate formation followed by ice formation at lower temperatures. Formation of each solid results in a visible distortion of the vapor bubble. In general, inclusions were cooled to -150°C ; usually, no solids other than ice and clathrate were recognized. However, solid CO_2 did form in the CO_2 -bearing inclusions in apatite (sample MT68-003-6) and also in ten inclusions in quartz from one sample of hydrous skarn (sample MT72-027-9). The characteristics of the inclusions that developed solid CO_2 will be discussed later.

In all the inclusions in quartz and garnet, and in several inclusions in pyroxene, the central carbonic phase exsolved into a liquid and vapor at low temperature ($T < 80^\circ\text{C}$). The homogenization of these phases (referred to as partial homogenization) occurs between -105° and -80°C . Histograms of partial homogenization temperatures (*T_{ph}*) are shown in Figure 4 for both anhydrous and hydrous skarn samples. Partial homogenization in most cases is to vapor, although several inclusions homogenize to liquid, and three by critical homogenization. With the exception of one inclusion each in pyroxene and garnet, partial homogenization to liquid is restricted to inclusions in quartz from hydrous skarn. The exsolution and the subsequent homogenization of this second fluid phase were not seen in many inclusions in pyroxene. These latter inclusions show double freezing and clathrate melting in the presence of a "vapor bubble." It is possible that the vapor phase is of such low density that an undetectably small amount of liquid is formed upon cooling below -80°C . As will be seen later, clathrate melting equilibria and *LRM* analyses are consistent with relatively low densities of the vapor in these inclusions. It is at least possible that the lower densities of inclusions in pyroxene compared to those in quartz and garnet result from the pyroxene's cleavage, which could allow fluid leakage.

Partial homogenization in the range -105° to -80°C and critical partial homogenization near

-82°C strongly suggest that methane is the dominant component in the "vapor" phase. However, the compositions and densities of the low-density fluid ("vapor" phase) in multicomponent systems are modified by the formation of clathrate and cannot be determined reliably from partial homogenization temperatures alone (e.g., Ramboz *et al.* 1985, Seitz *et al.* 1987). In particular, gas species that would be fractionated into the clathrate relative to the residual fluid, such as H_2S (Noaker & Katz 1954), may be present in significant concentrations and yet have little effect on the partial homogenization temperatures and pressures. However, they would affect the melting temperature of the clathrate.

In a few of the inclusions, critical homogenization occurs in the methane-rich fluid. This indicates fluid pressures near 46 bars (Fig. 5). As the temperature is raised, these same inclusions contain coexisting ice, clathrate, and a supercritical fluid. Under equilibrium conditions in the system $\text{H}_2\text{O}-\text{CH}_4$, the maximum allowable pressure for ice-clathrate-supercritical fluid coexistence is 24 bars (point A on Fig. 5). Under the assumption that isochores have at least a slightly positive slope in P - T space, there is a discrepancy in this apparent drop in pressure with increase in temperature (see Fig. 5). In part, this discrepancy may be because the actual fluids are not pure CH_4 - H_2O (e.g., dissolved NaCl). This observation also may indicate that the formation of clathrate in an inclusion frequently is a disequilibrium process (e.g., Brown & Lamb 1987). Brown & Lamb (1987) suggested that during rapid formation of clathrate, the enclathrated gas molecules may be derived principally from the gas fraction dissolved in the aqueous liquid, rather than from the gas present in the vapor bubble.

To test the latter hypothesis, we heated the inclusions to just below the clathrate melting temperature and cycled temperature up and down in the vicinity of (but below) this temperature. Upon further cooling at a very slow rate, the clathrate grows slowly, and either the methane-rich fluid does not exsolve into a liquid and vapor, or the resulting partial homogenization occurs at lower temperatures than under conditions of rapid cooling, consistent with the suggestions of Brown & Lamb (1987). Therefore, equilibrium amounts of clathrate may not form when inclusions are cooled quickly or without

-
- A. Low-magnification field of view of fluid inclusions in pyroxene from massive skarn (sample MT73-101-1). The area outlined by the dotted lines is enlarged in Fig. 3B. B. Primary fluid inclusions from the area enlarged from Fig. 3A. C. Low-magnification field of view of fluid inclusions in quartz from garnet skarn (sample MT72-043-6). The area outlined by the dotted lines is enlarged in Fig. 3D. D. Primary fluid inclusions in the area enlarged from Fig. 3C. Note that the field of view has been rotated clockwise $\sim 90^\circ$. E. Fluid inclusions in a garnet grain from garnet skarn (sample 73-101-3). F. Fluid inclusions in quartz from amphibole skarn (sample 72-028-2). G. Fluid inclusions in quartz from biotite skarn (sample 73-102-2). H. A fluid inclusion in quartz from garnet skarn (sample MTD-2) containing a hexagonal crystal of pyrrhotite(?). The crystal is identified as pyrrhotite because it gave no Raman spectrum corresponding to graphite and because it moved slightly when a magnet was placed in proximity.

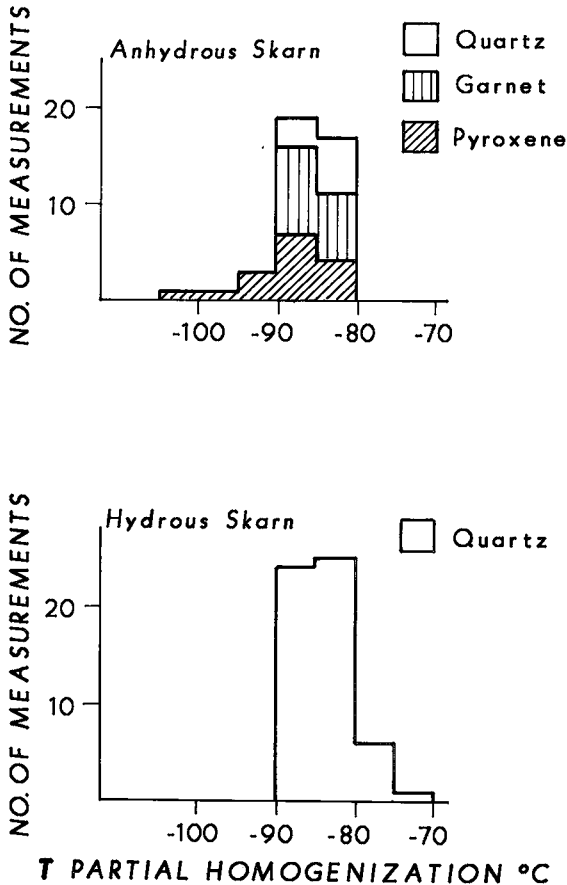


FIG. 4. Histograms of temperatures at which liquid and vapor methane homogenize into the low-density carbonic fluid ("vapor" bubble). These temperatures are referred to as partial homogenization temperatures (*T_{ph}*). In all but nine inclusions, this partial homogenization is to vapor. In the remaining nine inclusions, all of which are in quartz from hydrous skarn, six homogenize to liquid, and three experience critical homogenization.

very slow cooling combined with recycling procedures, and the resulting fluid pressure may be significantly higher than the corresponding equilibrium pressure based on curve 1 on Figure 5. Therefore, we attempted to approach equilibrium by cooling the inclusions very slowly, once the clathrate had formed. In spite of our attempts, the partial homogenization temperatures in Figure 4 may not always represent equilibrium conditions. However, these data are still useful in indicating that the low-density, carbonic fluid phase is CH₄-rich.

Salinities

Salinities in all inclusions are based on final

melting temperatures of ice (*Tim*) (Potter *et al.* 1978). Histograms of final melting temperatures of ice are shown in Figure 6 for both anhydrous and hydrous skarn samples. For inclusions in anhydrous skarn, *Tim* values range from -1.5°C to -6.0°C , which represent 3.0 to 8.5 equiv. wt.% NaCl. The mean temperature is -3.0°C , or 4.9 equiv. wt.% NaCl. Salinities are similar for inclusions in quartz, garnet and pyroxene. Melting temperatures of ice for inclusions in hydrous skarn range from -1.5°C to -7.0°C (3.0 to 9.0 equiv. wt. % NaCl). There seem to be two maxima in the histogram for hydrous skarn, near -2.5°C (4.0 equiv. wt. % NaCl) and -5.0°C (7.8 equiv. wt. % NaCl). Although there are significant variations in relative salinity within both the anhydrous and hydrous skarn (range: 3.0 to 9.0 equiv. wt.% NaCl), the average salinities are very similar for both skarn types (4.9 equiv. wt.% NaCl), indicating insignificant differences in salinity between the fluids responsible for anhydrous and hydrous skarn formation. As explained below, these salinities must be considered maxima because of the removal of H₂O from the liquid during clathrate formation (Collins 1979), the dissolved methane present in the aqueous liquid, and the elevation of pressure during ice melting in CH₄-H₂O inclusions compared to those during melting of pure H₂O (see Fig. 5; CH₄-H₂O inclusions are constrained to increase pressure along curve 1, in the presence of clathrate and ice, as temperature is increased).

In most inclusions, the first observation of melting occurred at temperatures that are obviously too high to represent a reasonable NaCl-water eutectic (*i.e.*, $< -10^{\circ}\text{C}$). However, in such low-salinity fluids, initial melting temperatures of ice are difficult to determine because little eutectic melt is produced. For the above inclusions, it was not possible to infer if solutes other than NaCl are present. However, in a few inclusions, the initial melting temperatures of ice are $< -20^{\circ}\text{C}$, which suggests that CaCl₂ and MgCl₂ may be present in addition to NaCl (Crawford 1981). Given the presence of hedenbergitic pyroxene and abundant pyrrhotite, FeCl₂ also may be an important additional component of the fluid. No initial melting temperatures of ice were observed between -10 and -20°C , which would have implied NaCl-KCl mixtures.

Melting temperatures of clathrate

Melting temperatures of clathrate were determined using the multistage cycling method of Ramboz *et al.* (1985) to overcome potential problems of disequilibrium during clathrate melting. Each inclusion was heated slowly until only a very small amount of the clathrate remained, then the inclusion was cooled 1–2 degrees. If the clathrate regrew (*e.g.*, became more visible), then the inclusion was heated

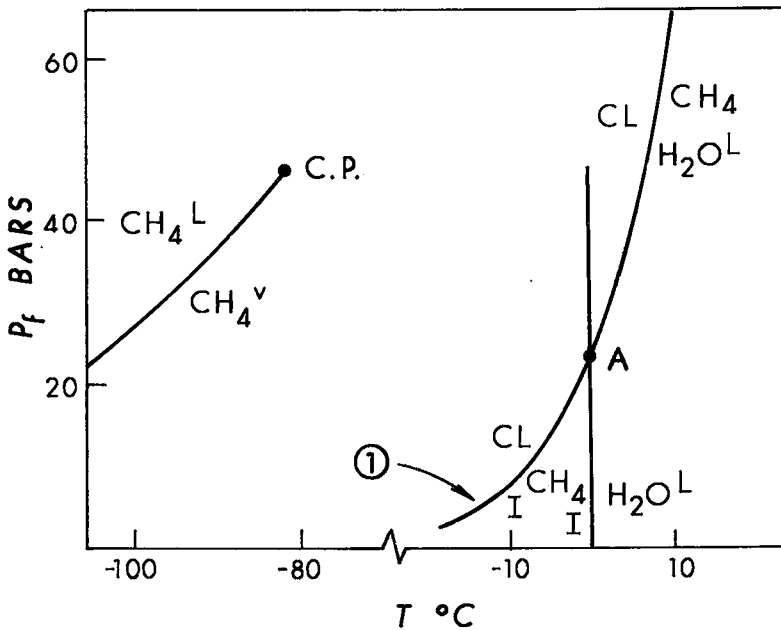


FIG. 5. Pressure-temperature diagram of selected equilibria in the system $\text{CH}_4\text{-H}_2\text{O}$, including those that define the stability of $\text{CH}_4\text{-H}_2\text{O}$ clathrates. The equilibria are from Deaton & Frost (1946), Marshall *et al.* (1964), Roo *et al.* (1983) and Miller (1985). The equilibrium pressure for coexistence of ice (I) -clathrate (CL)-methane fluid (CH_4) as a function of temperature is defined by curve 1; point A is the maximum pressure possible for this phase assemblage. This pressure is significantly lower than the critical pressure for methane.

0.1°C higher than previously and the process repeated until a temperature was reached at which clathrate did not grow on cooling. Clathrate melting temperatures determined in this way are very reproducible (generally within 0.2°C). We believe that this cycling method enhances the equilibration of clathrate with the coexisting fluid, thereby ensuring relatively accurate estimates of the melting temperature.

Histograms of clathrate melting temperatures (T_{cm}) are shown in Figure 7. For fluid inclusions in anhydrous skarn, T_{cm} ranges from 1.5° to 20.5°C . It is apparent from the histogram that inclusions in pyroxene generally have lower clathrate melting temperatures than inclusions in coexisting quartz and garnet, which could be due to selective leakage in pyroxene. The mean T_{cm} value for pyroxene falls between 10 and 11°C , and for garnet and quartz, between 15 and 16°C . For inclusions in hydrous skarn, T_{cm} ranges from 8.0 to 20.0°C , with the majority of the inclusions melting between 14 and 19°C .

Total homogenization

Total homogenization of the aqueous liquid and

CH_4 -rich carbonic fluid ("vapor bubble") leads to a liquid phase in all cases. Temperatures of total homogenization (T_{th}) are shown in Figure 8 for both anhydrous and hydrous skarn. Mean T_{th} values fall between 330° and 340°C for inclusions in pyroxene, and 350° to 360°C for inclusions in quartz. Inclusions in quartz and garnet commonly decrepitated prior to total homogenization, reflecting a high pressure of fluid in these inclusions.

Raman spectroscopic measurements

The temperatures of all observed phase changes are functions of fluid composition, density, and salinity. Owing to the potentially competing effects of these factors, microthermometry alone is insufficient to characterize accurately the composition of H-C-O-S-N fluids (Hollister & Burruss 1976, Burruss 1981). Laser Raman microprobe (LRM) analyses provide further compositional information on the carbonic fluid phase in 35 inclusions from one sample of anhydrous skarn (MT73-102-2) and four samples of hydrous skarn (MT72-027-9, MT72-027-10, MT72-028-7, and MT72-043-6).

The analyses show abundant CH_4 in all the analyzed inclusions, as had been inferred from their

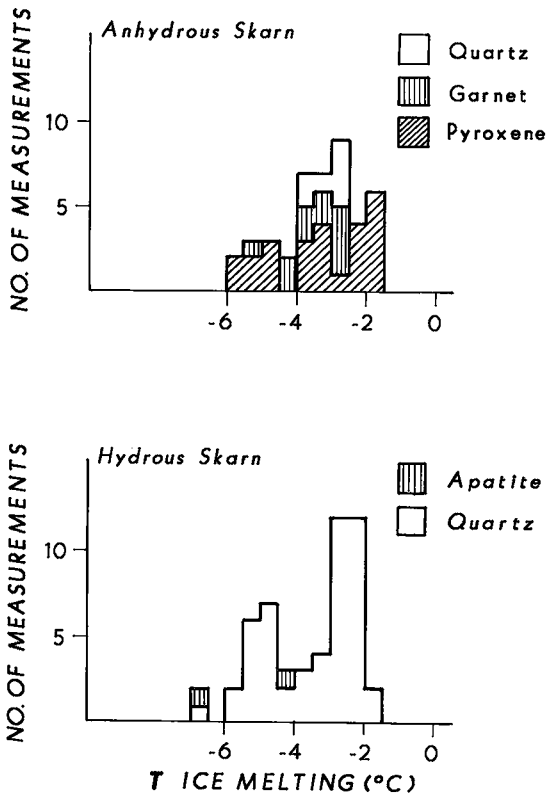


FIG. 6. Histograms of final melting temperatures of ice (T_m) in the presence of clathrate and $\text{CH}_4 - \text{H}_2\text{O}$ vapor.

low temperatures of partial homogenization. Hydrogen sulfide and nitrogen were detected as very minor components (approximately 2.5 mole % N_2 and 0.5 mole % H_2S measured in two inclusions in quartz from sample MT72-043-6 and about 5 mole % N_2 in two inclusions in pyroxene from sample MT73-102-2). Carbon monoxide, carbon dioxide, hydrogen, and higher hydrocarbons were sought, but not detected in any of the inclusions. In summary, the Raman analyses indicate that the carbonic phase in all the apparently primary inclusions is dominantly methane, with lesser, nearly trace, concentrations of nitrogen and hydrogen sulfide.

Raman analyses of several hexagonal, opaque crystals in fluid inclusions in quartz from sample MT-D-2 garnet skarn (Fig. 3H) show no graphite peaks (scanned spectral range $1200\text{--}1800\text{ cm}^{-1}$), although the LRM is a very sensitive indicator of graphite (e.g., Pasteris & Wopenka 1987). Slight movement of the opaque daughter crystal in one of these inclusions was observed when a magnet was moved around the microscope stage, which suggests that the daughter crystals are pyrrhotite. The Raman

spectrum of pyrrhotite is so weak that LRM analysis could not be used to confirm this identification. LRM analyses on the carbonic fluid in these same inclusions show them to be essentially pure CH_4 .

The detection limits of the LRM are estimated to be about 1 bar partial pressure for each of the volatiles CH_4 , H_2S , N_2 , and CO_2 (Wopenka & Pasteris 1987). For the inclusions analyzed in this study, the accuracy of the LRM analyses of the supercritical fluid is estimated to be about ± 3 mole % (absolute) for trace components, and for major components, about $\pm 10\%$ (relative) (Pasteris *et al.* 1988).

Fluid inclusions that generate a solid CO_2 phase

Six secondary inclusions in samples MT72-027-9 and -10 (a quartz vein cross-cutting pyroxene skarn) contain a solid phase that melts between -66° and -70°C . In these same inclusions, partial homogenization (all to vapor) occurs between -6° and -54°C , and clathrate melting occurs between 14.0° and 15.4°C . Measured salinities are higher in these six inclusions (av. = 8.0 equiv. wt. % NaCl) than in 8 other primary inclusions from these same samples that do not contain solid CO_2 (5.5 equiv. wt. % NaCl), possibly reflecting more dissolved CO_2 in the aqueous liquid in the former.

Raman microprobe analyses on the carbonic phase of these inclusions showed them all to be mixtures of CO_2 and CH_4 , ranging from approximately 53 to 82 mole % CH_4 . This is in agreement with the inference of Hollister & Burruss (1976), that for a $\text{CH}_4\text{--CO}_2$ carbonic phase in which melting of solid CO_2 occurs between -66° and -70°C , the CH_4 concentration must exceed 45 mole %. Four additional secondary inclusions showed melting phenomena suggestive of much higher CO_2 concentrations. LRM analyses confirmed this, showing a tight cluster of compositions around 14 ± 1 mole % CH_4 , 86 ± 1 mole % CO_2 .

Solid CO_2 was observed at low temperatures in inclusions in apatite crystals in sample MT68-003-6. The inclusions contain approximately 45–50 vol. % vapor at 30°C . These inclusions are characterized by the melting of solid CO_2 between -59 and -60°C , T_{cm} values between 9.5° and 10.0°C , and T_{ph} (to vapor) between $+26.5^\circ$ and $+28^\circ\text{C}$. These temperatures of CO_2 melting and partial homogenization indicate that there must be at least one more species in addition to CO_2 and CH_4 in the inclusions (Heyen *et al.* 1982), and that this additional species has a triple point below that of CO_2 but a critical temperature above that of CO_2 . One of the few reasonable volatiles to fulfill the latter criterion is H_2S . Attempts were made to analyze quantitatively these CO_2 -rich inclusions. However, the natural fluorescence of apatite under the laser beam

precluded analysis by *LRM*. Inclusions in the surrounding quartz are the methane-bearing, high-*T_{cm}* inclusions typical of hydrous skarn. Although the quartz and apatite appear to be contemporaneous, the inclusions in apatite are not obviously primary, based on their characteristics and textural relationships. Their origin is unclear; these inclusions deserve further study.

DISCUSSION

Clathrate melting equilibria

Clathrate melting temperatures are functions of fluid composition, density and salinity. A full evaluation of the effect of salinity on clathrate melting temperature is complicated by the fact that salinities are estimated from ice-melting temperatures (*Tim*); in our inclusions, ice melts in the presence of clathrate. The salinities inferred from *Tim* values, therefore, must be maxima because of the removal of water during clathrate formation. Based on the molar volumes of clathrate (von Stackelberg & Mueller 1954) and H₂O-NaCl solutions (Potter & Brown 1977), 25 vol. % of an NaCl aqueous solution must be converted to clathrate to increase the salinity from 4 to 5 wt.%. In the inclusions under study, the clathrate forms a shell around the vapor phase. Although there are large uncertainties in estimating its volume proportions, the clathrate generally occupies far less than 10% of the volume of the liquid and thus does not contribute more than about 0.4 wt.% to the apparent salinity.

The presence of methane vapor raises the pressure in the inclusion substantially above 1 bar and lowers the freezing point of pure water (see Fig. 5); this results in a further overestimate of salinities based on *Tim*. Critical partial homogenization of the methane liquid and vapor at -82°C corresponds to 46 bars pressure, whereas the equilibrium pressure of ice melting in the presence of CH₄-clathrate and supercritical CH₄ fluid is 24 bars (discussed above). This difference suggests that the actual minimum pressure in the inclusion during ice melting was about 40 bars, which would correspond to a temperature decrease of 0.3°C (Hanor 1980), or an apparent salinity increase of 0.3 wt.% NaCl (*LRM* data on the inclusions at room temperature indicate internal pressures from about 65 to 220 bars, as discussed below). The dissolution of gas species in water also would lower the melting temperatures of ice (Hedenquist & Henley 1985), but the low solubility of CH₄ in H₂O-NaCl solutions makes this a minor effect. Maximum solubility of methane at these *P-T* conditions is roughly 1000 ppm or 0.09 molal (Hanor 1980) which, based on the relationship of Hedenquist & Henley (1985), *i.e.*, $T = 1.86 \times M$ (*M* = molal), corresponds to a temperature decrease

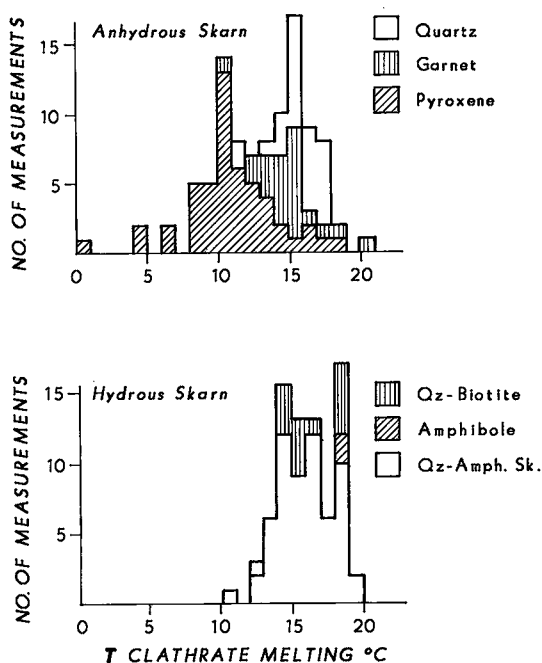


FIG. 7. Histograms of clathrate melting temperatures (*T_{cm}*).

of <0.1°C. Because all of the inclusions have similar volatile contents and a similar range of salinities, the above factors are believed to have affected their apparent salinities in roughly the same way. Based on all of these considerations, we estimate that measured salinities in most of the inclusions are not more than 0.5 wt.% higher than true salinities.

The effect of dissolved NaCl on CH₄-clathrate stability has been determined by Roo *et al.* (1983). For a temperature range of -12.30° to 12.83°C and pressures up to 110 bars, they arrived at the following expression:

$$\ln(P) = -8160.43/T + 33.1103 - 128.65X + 40.28X^2 - 138.49\ln(1-X)$$

where *P* is the pressure in bars, *T* is temperature in Kelvin, and *X* is the mole fraction of NaCl in the liquid phase on a methane-free basis. Based on this expression, the isobaric depression of the methane-clathrate melting curve for 3.0 and 5.0 wt. % NaCl solutions is 1.0° and 1.9°C, respectively.

The average 5°C difference between *T_{cm}* values from pyroxene (anhydrous skarn) and quartz (garnet or hydrous skarn) would require a minimum salinity difference of 10 wt. % NaCl by the above calculations. However, *Tim* values in these same inclusions show a maximum difference of only 4 wt. %

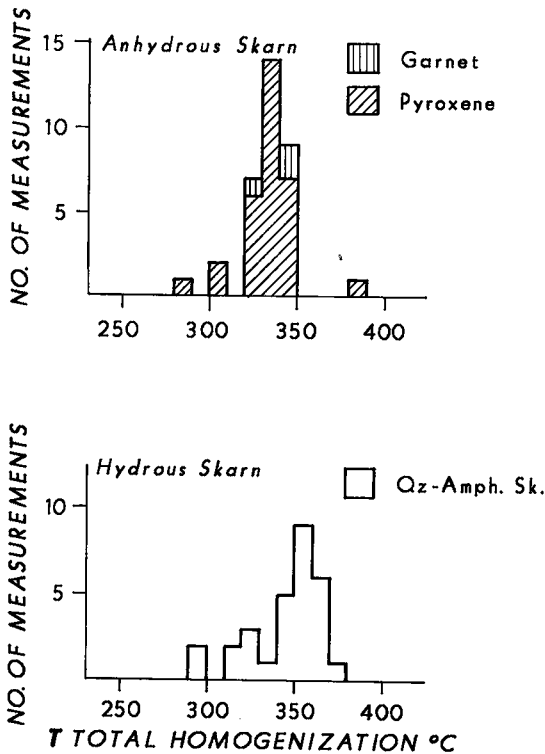


FIG. 8. Histograms of total homogenization temperatures (T_{th}).

NaCl. In fact, the minimum difference in salinity inferred to account for the range in clathrate melting temperatures is much higher than the total salinity measured in inclusions in either pyroxene or quartz. Furthermore, there is no strong correlation between T_{im} and T_{cm} values for these inclusions. Therefore, variable salinity cannot be the primary factor responsible for the general increase of T_{cm} values from early pyroxene skarn to later hydrus skarn. Another explanation must be sought for the variation in clathrate melting temperatures. Pressure is another variable that affects T_{cm} , even among inclusions of essentially the same composition.

Raman spectroscopic data are a particularly useful complement to microthermometric data, because the exact spectral position of the Raman peak for CH_4 is a function of the fluid pressure (May *et al.* 1959, Fabre & Couty 1986). Thus, Raman analysis provides an independent check on the total internal pressure in CH_4 -bearing inclusions. In this study, the Raman peaks for CH_4 occur at approximately 2915 cm^{-1} for five inclusions analyzed in pyroxene from sample MT73-101-1 (av. T_{cm} 10°C), and at 2912 cm^{-1} for five inclusions in quartz from sample MT72-043-6 (hydrus skarn, av. T_{cm} 18°C), with a combined sample variation and uncertainty of 1 cm^{-1} in the

actual peak position (calibrated against an Ar vapor lamp). These spectral positions represent estimated fluid pressures of 220 ± 50 bars at 25°C for the inclusions in hydrus skarn and 65 ± 20 bars for inclusions in pyroxene skarn (Fabre & Couty 1986). Even with their associated large uncertainties, the Raman peak positions for CH_4 clearly indicate that pressure is lower in inclusions from early, anhydrous skarn compared to those from later, hydrus skarn. Therefore, the increase in average T_{cm} value from anhydrous to hydrus skarn probably results from changes in density, not bulk composition. We assume that these density differences are primary, but leakage along cleavage planes in pyroxene cannot be ruled out. Higher vapor densities in inclusions with the higher T_{cm} values also are consistent with the phase changes observed during partial homogenization. In inclusions with the highest values of T_{cm} (hydrus skarn), partial homogenization is frequently to liquid, whereas in inclusions with lower values of T_{cm} (early anhydrous skarn), partial homogenization is to vapor. It is also interesting to note that LRM data show the internal pressures in both the CH_4 and CH_4 - CO_2 carbonic fluids in inclusions from samples MT72-027-9 and -10 (hydrus skarn) to be about the same, *i.e.*, 130 ± 25 bars.

Estimates of $X(CH_4)$, P and T

In order to determine the molecular proportions of CH_4 and H_2O , and to construct isochores for pressure corrections to final homogenization temperatures, it is necessary to determine the molar volumes of the methane-rich fluid ($\bar{V}(CH_4)$) and aqueous liquid (\bar{V}_a). Commonly, the molar volume of the carbonic fluid phase is determined from T_{ph} (Mullis 1979) or T_{cm} (Ramboz *et al.* 1985). However, the molar volume of the total carbonic fluid may be affected by the presence of ice and clathrate (Ramboz *et al.* 1985, Seitz *et al.* 1987), thus precluding the use of partial homogenization temperatures for determining molar volumes of the carbonic fluid in the inclusions from MacTung.

Parry (1986) developed an iterative method of determining thermodynamically consistent values of P and $X(CO_2)$ at the homogenization temperature for the CO_2 - H_2O -NaCl system. An analogous approach for the CH_4 - H_2O -NaCl system is not possible for fluids with $X(CH_4) < 0.10$ owing to the present lack of experimental two-phase boundary curves (isothermal liquid + vapor to liquid curves in P - X space) in this region. Addition of even small amounts (< 1 mole %), of NaCl greatly increases the two-phase (CH_4 -vapor and aqueous liquid) region (Krader & Franck 1986). Thus, application of Parry's method to the two-phase boundary curves for the salt-free CH_4 - H_2O system significantly overestimates $X(CH_4)$ and underestimates pressure.

Therefore, in this study, values of $X(\text{CH}_4)$, $\bar{V}\text{CH}_4$, and $\bar{V}(\text{bulk})$ were calculated by estimating the fraction of the inclusion occupied by carbonic fluid (fcv) at the clathrate melting temperature. These estimates were made for each analyzed inclusion by measuring the dimensions of the inclusion and vapor bubble on the microscope stage. For a representative set of inclusions from each skarn type, these estimates were refined by making measurements on enlarged photographic prints of a number of inclusions by calculating area fractions (e.g., two dimensions) of fluid with counting grids. These area fractions were then converted to volume fractions (fcv) by generating closed cylinders (for inclusions) or spheres (for bubbles of carbonic fluid) from the rotation about the long axis of the two-dimensional shapes seen in section. In order to minimize the effect of the presence (e.g., amount) of clathrate on the molar volume of the methane-rich fluid, the measurements or photographs were always taken just before the clathrate disappeared. Estimates of fcv are precise (estimated 3% error maximum in area fractions) using these methods, based on repetitive measurements of single inclusions and of multiple inclusions within restricted areas of single grains. The high precision is probably enhanced by the comparative homogeneity and fairly regular shapes of the inclusions. However, the accuracy of the fcv estimates must be less than the precision because of the poorly known effects of inclusion shape in the third dimension. Parry (1986) has pointed out that as much as 50% error can occur in the estimate of $P(\text{CO}_2)$ by extrapolating two-dimensional area fractions in irregularly shaped inclusions into the third dimension. By measuring carefully area fractions in inclusions having similar proportions and composition of phases as well as relatively regular shape, we believe that the uncertainties in the fcv values are no worse than $\pm 10\%$. Because the sizes, shapes, and compositions of the fluid inclusions are similar in all four skarn facies, any systematic errors are likely to occur in the same direction and be of similar magnitude for each of the skarn facies.

The above procedure yields volumetric ratios of aqueous liquid and carbonic fluid at the melting temperature of clathrate. Owing to the relative incompressibility of H_2O , the temperature of analysis and the salinity (measurement described earlier) are sufficient to define the molar volume of the aqueous phase (Potter & Brown 1977). For the supercritical CH_4 fluid phase (purity confirmed by LRM), the pressure of clathrate melting (at the measured temperature) can be estimated by reference to the equilibrium CH_4 -clathrate phase diagram (Marshall *et al.* 1964), corrected for the effects of salinity (Roo *et al.* 1983). The molar volume of CH_4 at this T and P is derived from an equation of state for CH_4 (Jacobs & Kerrick 1981).

If the molar volumes of the CH_4 -fluid ($\bar{V}\text{CH}_4$) and aqueous liquid ($\bar{V}a$) are known, along with fcv , the mole fraction of methane can be determined from:

$$X(\text{CH}_4) = fcv/\bar{V}\text{CH}_4 + [fcv/\bar{V}\text{CH}_4 + (1-fcv)/\bar{V}a].$$

Then $\bar{V}(\text{bulk})$ can be calculated from:

$$\bar{V}(\text{bulk}) = X(\text{CH}_4)\bar{V}(\text{CH}_4) + [1 - X(\text{CH}_4)]\bar{V}(a).$$

Two minor contributions to the value of $X(\text{CH}_4)$ have been ignored. The very small solubility of CH_4 in H_2O at about 15°C and 40 bars (Bonham 1978) permits the assumption that all the CH_4 in an inclusion is contained in the carbonic fluid. Since the phase-volume estimates are based on the presence of negligible amounts of clathrate, one also can neglect the trace amount of CH_4 that is tied up in the clathrate.

Calculated values of $X(\text{CH}_4)$ range from 0.005 to 0.02 in inclusions from pyroxene and from 0.01 to 0.04 in inclusions from garnet and quartz. After $\bar{V}(\text{bulk})$ and $X(\text{CH}_4)$ were determined, isochores were calculated using the hard-sphere modified Redlich-Kwong equation of state developed for CH_4 - H_2O fluids by Jacobs & Kerrick (1981) and Kerrick & Jacobs (1981). The isochores are extremely sensitive to estimates of fcv , and an uncertainty of $\pm 20\%$ in its value yields an uncertainty of approximately ± 400 bars in the isochore. This error, along with the uncertainties in molar volumes of the CH_4 -fluid and the effect of NaCl on the isochores, contribute to significant uncertainties in estimates of temperature ($\pm 30^\circ\text{C}$) and pressure (± 500 bars) from the isochores. Unfortunately, improvement in these uncertainties must await additional experimental data on two-phase boundary curves (isothermal liquid + vapor to liquid boundaries in P - X space) in the H_2O -rich portion of the NaCl - H_2O - CH_4 system (see discussion above).

The average isochores derived from the inclusions are shown for each skarn type in Figure 9. These originate at the minimum temperature and fluid pressure defined by the average final homogenization temperature (T_{th}) and average calculated density for each facies. The average isochores for garnet and amphibole skarns are virtually identical, whereas the average isochore for inclusions in pyroxene is about 50°C higher (or 600 bars lower). The average isochore for the biotite skarn is offset about 25°C lower (or 350 bars higher) than those for the garnet and amphibole skarns. Thus the average density of trapped fluids in the pyroxene skarns is somewhat less, and the average density of trapped fluids in the biotite skarns somewhat more, than that of fluids in both the garnet and amphibole skarns. The Raman-derived pressure data at room temperature

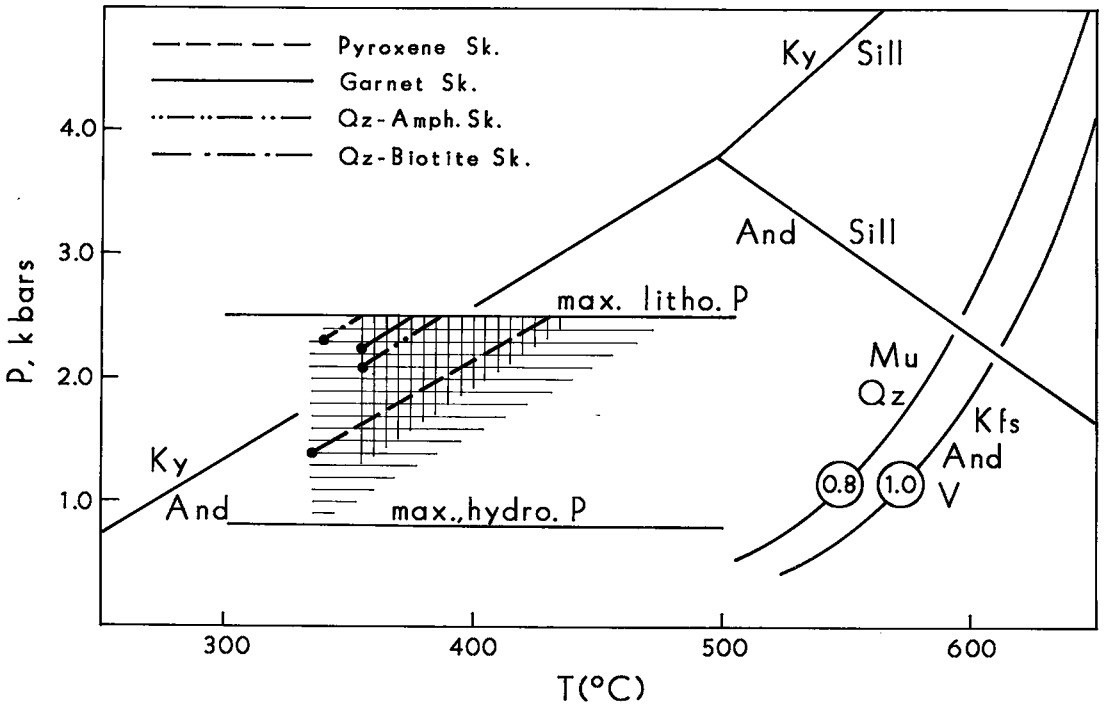


FIG. 9. P - T diagram illustrating average isochores for inclusions in pyroxene, garnet, amphibole, and biotite skarns. These originate at the minimum temperature and fluid pressure (solid circles) defined by the average total homogenization temperature (T_{th}) and average calculated density for each skarn facies: pyroxene skarn ($T = 335^{\circ}\text{C}$, $P = 1.4$ kbars); garnet skarn ($T = 355^{\circ}\text{C}$, $P = 2.2$ kbars); amphibole skarn ($T = 355^{\circ}\text{C}$, $P = 2.1$ kbars); biotite skarn ($T = 340^{\circ}\text{C}$, $P = 2.3$ kbars). Because of variations in T_{cm} and f_{cv} values within skarn facies, there is considerable overlap in the ranges of calculated isochores between skarn facies, as illustrated for the pyroxene (horizontal line pattern) and garnet (vertical line pattern) skarns. The occurrence of andalusite + K-feldspar in metapelites defines upper limits to lithostatic pressure for contact metamorphism and skarn formation. The phase equilibria relevant to andalusite + K-feldspar stability are from Holdaway (1971) and Kerrick (1972). Allowing for the possibility for fluid pressure less than total pressure (e.g., $0.8 P_T$), the likely maximum lithostatic or total pressure for the contact aureole is 2.5 kbars. The maximum likely hydrostatic pressure for this total (load) pressure also is shown.

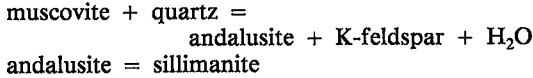
also support the relative positions of the isochores; that is, at room temperature, the inclusions in pyroxene skarn are at lower pressure than are the inclusions from garnet and hydrous skarn. We assume that these density differences are primary, but leakage along cleavage planes in pyroxene cannot be ruled out. If post-entrapment leakage in pyroxene did occur, then the primary differences in density between inclusions in pyroxene and those in quartz and garnet will be less than the measured differences. Accordingly, the differences between the P - T locations of isochores calculated for the pyroxene facies and those calculated for the other skarn facies (Fig. 9) should be regarded as maxima.

There are significant variations in the densities (e.g., P - T locations of isochores) calculated for individual inclusions within each facies, as indicated for the pyroxene and garnet skarns by the horizontal and vertical lining, respectively (Fig. 9). The var-

iations in calculated density *within* individual skarn facies are large compared to the average difference in calculated density *between* skarn facies. Hence there is a significant degree of overlap for fields of isochores between skarn types. In particular, the range of isochores for pyroxene skarn overlaps the average isochores for garnet and amphibole skarns (Fig. 9). Also, the range of isochores calculated for biotite skarn (not shown in Fig. 9) overlaps the range of isochores for both garnet and amphibole skarns. Based on these average calculated isochores and measured temperatures of final homogenization, minimum temperatures and pressures of entrapment for the various types of skarn are: pyroxene skarn: $T = 335^{\circ}\text{C}$, $P = 1.4$ kbars; garnet and amphibole skarn: $T = 355^{\circ}\text{C}$, $P = 2.1$ kbars, and biotite skarn: $T = 340^{\circ}\text{C}$, $P = 2.3$ kbars. These minimum pressures, especially those for garnet, amphibole and biotite skarns, are consistent with Newberry's (1982)

contention that tungsten skarns typically form at significant depth (5–10 km).

The occurrence of andalusite + K-feldspar in metapelites in the thermal aureole of the MacTung stock defines upper limits to lithostatic pressure during contact metamorphism and skarn formation by the intersection of the reactions (Fig. 9):



At $P(\text{H}_2\text{O}) = P_T$, this upper P limit is 2.2 kbars (Holdaway 1971, Kerrick 1972). Even considering the possibility that $P(\text{H}_2\text{O})$ might be somewhat less than P_T (for example, 0.8 of P_T) in the metapelites within the thermal aureole, the upper limit to P_T is likely to be no higher than 2.5 kbars (Fig. 9). The equivalent maximum hydrostatic pressure for the overburden also is shown in Figure 9.

Comparison of these maximum limits to the locations of the isochores for garnet, amphibole and biotite skarns indicates that homogenization pressures are high (>2.0 kbars for most samples of amphibole and garnet skarns and all samples of biotite skarns); thus fluid pressures (P_f) closely approached lithostatic pressure during development of the garnet, amphibole, and biotite skarn facies. The minimum estimate for fluid pressure is lower for pyroxene skarn formation (1.4 kbars). However, pyroxene skarn formation at P_f significantly less than lithostatic pressure is possible only if fluid pressures significantly increase during subsequent stages of skarn development (e.g., development of garnet and hydrous skarn). Assuming that this did not occur, then fluid pressure throughout skarn evolution is limited to greater than 2.1 kbars (the minimum fluid pressure during garnet, amphibole and biotite skarn formation) and less than 2.5 kbars (the maximum load pressure possible for the contact aureole). Although these limits are significantly above hydrostatic conditions, it is possible, even likely, that fluid pressure fluctuated between these limits (e.g., between 2.1 and 2.5 kbars) throughout skarn development. Textures in the MacTung skarns (Figs. 2A, B, C) provide evidence for fracturing and subsequent crack sealing by precipitation of quartz. Repetitive fracturing and re-sealing by quartz precipitation provide a ready and plausible means of producing such limited fluctuations in fluid pressure.

The fluid-inclusion data from MacTung provide quantitative estimates of fluid density and variations in fluid density at entrapment. Because density is a function of both T and P , these variations in density do not automatically require equivalent variations in temperature. However, the simplest interpretation of the variations in density (e.g., different locations of the isochores) is that skarn formation

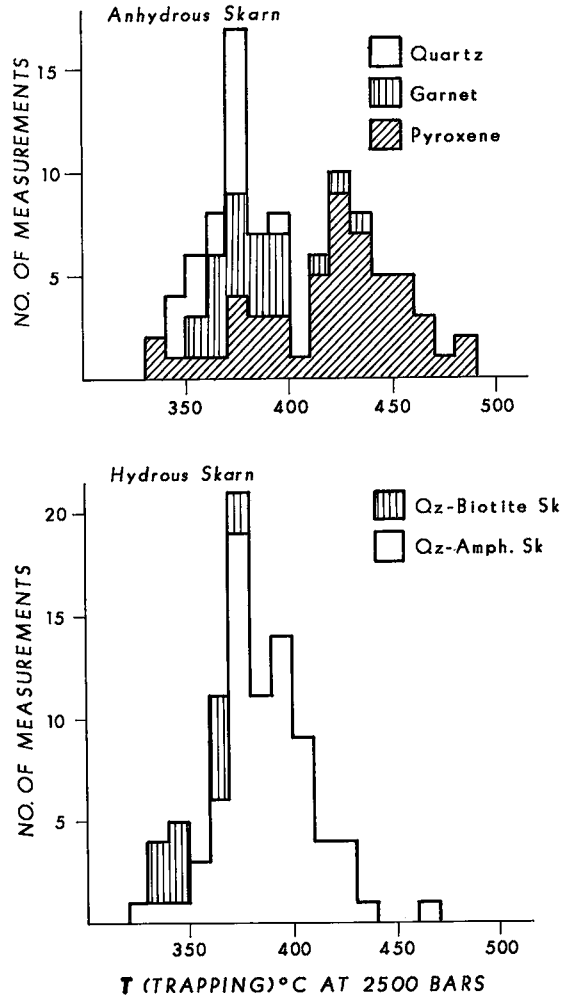


FIG. 10. Histograms of trapping temperatures based on a likely maximum fluid pressure of 2.5 kbars.

occurred over a range of temperature at constant P_f . This interpretation maximizes the temperature variations required at entrapment because it requires variations in temperature to be responsible for the total range of density recorded by the fluid inclusions. At a constant fluid pressure of 2.5 kbars, temperature must vary between 480 and 330°C to explain the total variation in density recorded by all the fluid-inclusion measurements. However, even the modest pressure fluctuations inferred above for entrapment (2.1 to 2.5 kbars) would reduce significantly the temperature variation required to explain all variations in density recorded by the fluid-inclusion measurements to about 100°C or between 445 and 345°C. It is also worth noting here that *all* variations in density recorded by fluid inclusions at MacTung could

be accounted for at *constant* temperature (about 345°C) if fluid pressure at entrapment fluctuated between 1.0 and 2.5 kbars (*e.g.*, between hydrostatic and lithostatic pressure). In such a situation the early pyroxene skarn must form at systematically lower fluid pressure (about 1.5 kbar average) than the later skarn types (≤ 2.1 kbar average).

Assuming a maximum and constant pressure of 2.5 kbars for intrusion, contact metamorphism, and skarn formation, maximum entrapment or formation temperatures have been calculated for the skarn facies (Fig. 10). We emphasize that these results record maximum possible variations in temperature for skarn formation. The pyroxene skarn began forming at temperatures of 480°C and continued to form to temperatures as low as 339°C, a temperature range equivalent to that recorded by inclusion data from all skarn types at MacTung. If temperature can be equated with time, then the implication of this variation in temperature is that pyroxene skarn formed throughout skarn development at MacTung. The bulk of the pyroxene skarn formed over the restricted temperature range of 470°C to 410°C. Again assuming constant fluid pressure, pyroxene skarn formed about 50°C higher, on average, than the next two stages, garnet and amphibole skarns. However, some of the pyroxene skarn formed at *P-T* conditions virtually identical to those of the succeeding garnet and amphibole skarns (Fig. 10). The average isochores defined for amphibole skarn (inclusions in quartz) and for garnet skarn (inclusions in both garnet and quartz) plot at very similar temperatures at any given *P* (380°C at 2.5 kbars), indicating very similar conditions of entrapment, and implying very little elapsed time between formation of the initial (hydrous) and late (anhydrous) skarn. The bulk of both garnet and amphibole skarn formed over the temperature range of 430 to 350°C. Much of the formation of biotite skarn occurred at lower temperatures, as indicated by its average isochore, which plots about 30°C lower than the average isochore for amphibole skarn. However, at least some of the biotite skarn formed at *P-T* conditions virtually identical to those ($P > 2.0$ kbars; $350^\circ < T < 375^\circ\text{C}$) characterizing the latest pyroxene skarn and the latter parts of both garnet and amphibole skarn.

SUMMARY

Microthermometric and laser Raman microprobe analyses of fluid inclusions indicate that the skarn-forming fluid at MacTung was primarily a binary $\text{H}_2\text{O}-\text{CH}_4$ fluid. The calculated $X(\text{CH}_4)$ values in the skarn fluid increase from pyroxene skarn ($0.005 \leq X(\text{CH}_4) \leq 0.02$) to hydrous skarn ($0.01 \leq X(\text{CH}_4) \leq 0.04$). Laser Raman microprobe ana-

lyses indicate that the skarn fluid contains traces (approximately 0.5 and 2–3 bars partial pressure, respectively) of H_2S and N_2 , whereas concentrations of carbon dioxide, carbon monoxide, hydrogen, and higher hydrocarbons are below detection limits (< 1 bar partial pressures) in the primary fluid inclusions. Salinities are low (in general < 5 wt. % NaCl equivalent) and do not vary significantly from early anhydrous to later hydrous skarn. In a few cases, the observed initial melting temperatures of ice (-32 to -20°C) suggest that some of the fluids contain either CaCl_2 or MgCl_2 , in addition to NaCl.

The fluid-inclusion data indicate that the skarn fluids at MacTung are remarkably reduced, with virtually all carbon as CH_4 . The inference of a highly reduced fluid is consistent with the presence of hedenbergitic pyroxene and andradite-poor garnet (Dick 1976).

Temperature estimates based on fluid-inclusion analyses indicate that formation of pyroxene skarn began at temperatures close to 480°C, the greater part of it forming in the temperature range 410 to 470°C. The remainder of the anhydrous skarn (some pyroxene skarn and most garnet skarn) and the initial hydrous skarn (amphibole skarn) then developed in the common temperature range 360–415°C, at maximum pressure of about 2.5 kbars. This equivalence in the *P-T* conditions of entrapment suggests that the garnet and amphibole skarns formed over the same, or similar, time intervals. Both anhydrous (garnet-quartz) and hydrous assemblages continued to form as temperature fell. The biotite skarn (latest stage) formed between 330 and 385°C. The majority of each skarn type formed over a limited range of temperature ($< 60^\circ\text{C}$). The development of the initial hydrous skarn and some of the anhydrous skarn occurred at very similar temperatures; there is little evidence that hydrous skarn formation was exclusively retrograde or that "retrograde" or hydrous skarn formation was initiated primarily by falling temperature. The similarity in temperatures of formation between some of the pyroxene skarn and virtually all of both garnet and amphibole skarn is consistent with their essentially simultaneous development along with zoned calc-silicate hornfels, as proposed by Dick & Hodgson (1982). Mathieson & Clark (1984) reached similar conclusions for the development of the analogous suite of skarn facies in the CanTung tungsten skarn. In detail the bulk of the pyroxene skarn at MacTung formed at somewhat higher temperature (50°C higher, on average) than the bulk of garnet and amphibole skarns, *if* all skarn types formed at the same fluid pressure. The subsequent drop in temperature associated with continued formation of hydrous skarn at MacTung is not as large as the decrease in temperature recorded in the CanTung skarn deposit (Mathieson & Clark 1984). The maximum drop in temperature ($< 150^\circ\text{C}$)

between development of highest-temperature anhydrous and latest (*e.g.*, lowest-temperature) hydrous (biotite) skarn in the MacTung deposit is also much less than that proposed for the analogous skarn evolution in the Pine Creek tungsten skarn (Newberry 1982, Brown *et al.* 1985), or in several Cu-skarn deposits (Eastoe 1978, Ahmad & Rose 1980, Cook 1982, Shelton 1983, Kemp 1985, Connelly & Bowman 1990).

The fluid-inclusion data indicate that some variations in temperature and probably fluid pressure occurred within skarn types and that total development of the skarn took place over a range of temperature, probably not exceeding 100°C. The data further indicate that there was no significant break in the *P-T* conditions between anhydrous and hydrous skarn formation; there is significant overlap in formation temperatures for all skarn facies. The bulk of both anhydrous (garnet) skarn and hydrous (amphibole) skarn formed at equivalent temperatures and pressures (along equivalent isochores). The data also indicate load pressures of 2.1–2.5 kbars. These pressures are consistent with the range of depths (5–10 km) suggested for the formation of tungsten skarn in general by Newberry (1982), but are greater than the 1.0 kbar estimate at CanTung on the basis of sphalerite geobarometry (Mathieson & Clark 1984). Furthermore, fluid pressures remained high (>2.0 kbars) throughout formation of all skarn facies; the development of hydrous skarn was not accompanied by a drop in fluid pressure from near lithostatic to hydrostatic conditions, as proposed for skarn formation in general by Einaudi *et al.* (1981). The evidence from both textural relationships and fluid-inclusion data suggests that from one location to another within the MacTung deposit, *all* skarn facies were forming over a limited range of *P-T*; at any specific location and time, a single skarn facies could form at somewhat different *P-T* conditions.

The detailed *P-T* regime of the MacTung skarns does not correspond closely to that proposed by Einaudi *et al.* (1981) as typical of skarn development in general nor to that proposed by Newberry (1982) as typical of tungsten skarn development in particular. Specifically, the data from MacTung do not support models of tungsten skarn formation in which an early, exclusively anhydrous stage forms at high temperature and high (*i.e.*, lithostatic) pressure and is followed by a later, hydrous stage, which forms at distinctly lower temperature and lower (*e.g.*, hydrostatic) pressures. Temperature and pressure are not the sole variables responsible for the mineralogical variations and scheelite deposition at MacTung. Chemical variables have an important but as yet undetermined role in the formation of this skarn deposit. Their importance will be the subject of the next part of this study.

ACKNOWLEDGEMENTS

We gratefully acknowledge AMAX Northwest Mining Company Limited for access to the MacTung property, for logistical support at the site, and for permission to sample drill core. In particular, we thank both Dorothy Atkinson and Don Baker for the generous amount of time and advice they provided concerning the geology and petrology of the deposit. This study would not have been possible without their assistance. We thank Alan Clark, Jeffery Seitz, and Anthony E. Williams-Jones for review of the manuscript. This study was partially supported by the National Science Foundation through grant EAR 81-07551 to JRB and grant EAR 8708123 to JDP. Donna Thomas and Sheila Merrill kindly typed the manuscript.

REFERENCES

- AHMAD, S.N. & ROSE, A.W. (1980): Fluid inclusions in porphyry and skarn ore at Santa Rita, New Mexico. *Econ. Geol.* **75**, 229-250.
- BONHAM, L.C. (1978): Solubility of methane in water at elevated temperatures and pressures. *Am. Assoc. Petrol. Geol. Bull.* **62**, 2478-2488.
- BOWMAN, J.R., COVERT, J.J., CLARK, A.H. & MATHIESON, G.A. (1985): The CanTung E-zone scheelite skarn ore body, Tungsten, Northwest Territories: oxygen, hydrogen, and carbon isotope studies. *Econ. Geol.* **80**, 1872-1895.
- BROWN, P.E., BOWMAN, J.R. & KELLY, W.C. (1985): Petrologic and stable isotope constraints on the source and evolution of skarn forming fluids at Pine Creek, California. *Econ. Geol.* **80**, 72-95.
- _____ & LAMB, W.M. (1987): Estimation of mole fraction CO₂ and pressure in fluid inclusions—an improved graphical approach *Geol. Soc. Am., Abstr. Programs* **19**, 603.
- BURRUSS, R.C. (1981): Analysis of phase equilibria in C-O-H-S fluid inclusions. In *Fluid Inclusions: Applications to Petrology* (L.S. Hollister & M.L. Crawford, eds.). *Mineral. Assoc. Can. Short Course Handbook*, **6**, 39-74.
- BURT, D.M. (1971a): Some phase equilibria in the system Ca-Fe-Si-C-O. *Carnegie Inst. Wash. Year Book* **70**, 178-184.
- _____ (1971b): The facies of some Cu-Fe-Si skarns in Japan. *Carnegie Inst. Wash. Year Book* **70**, 185-191.
- COLLINS, P.L.F. (1979): Gas hydrates in CO₂-bearing fluid inclusions and the use of freezing data for estimation salinity. *Econ. Geol.* **74**, 1435-1444.

- CONNELLY, M.P. & BOWMAN, J.R. (1990): Petrologic, fluid inclusion, and stable isotope constraints on the physicochemical evolution and origin of skarn-forming fluid, Bwana and Maria copper skarns, Milford, Utah. *Econ. Geol.* (in press).
- COOK, S.J. (1982): *The Physical-Chemical Conditions of Contact Skarn Formation at Alta, Utah*. M.S. thesis, Univ. of Utah, Salt Lake City, Utah.
- CRAWFORD, M.L. (1981): Phase equilibria in aqueous fluid inclusions. In *Fluid Inclusions: Applications to Petrology* (L.S. Hollister & M.L. Crawford, eds.), *Mineral. Assoc. Can., Short Course Handbook 6*, 75-100.
- DEATON, W.M. & FROST, E.M., JR. (1946): Gas hydrates and their relation to the operation of natural gas pipelines. *U.S. Bur. Mines, Monogr. 8*.
- DICK, L.A. (1976): *Metamorphism and Metasomatism at the MacMillan Tungsten Deposit, Yukon and District of Mackenzie, Canada*. M.Sc. thesis, Queen's Univ., Kingston, Ontario.
- _____ & HODGSON, C. J. (1982): The MacTung W-Cu(Zn) contact metasomatic and related deposits of the northeastern Canadian Cordillera. *Econ. Geol.* **77**, 845-867.
- EASTOE, C.J. (1978): A fluid inclusion study of the Panguna porphyry copper deposit, Bougainville, Papua New Guinea. *Econ. Geol.* **73**, 721-748.
- EINAUDI, M.T., MEINERT, L.D. & NEWBERRY, R.J. (1981): Skarn deposits. *Econ. Geol., 75th Anniv. Vol.*, 317-391.
- FABRE, D. & COUTY, R. (1986): Étude, par spectroscopie Raman, du méthane comprimé jusqu'à 3 kbar. Application à la mesure de pression dans les inclusions fluides contenues dans les minéraux. *C.R. Acad. Sci. Paris* **303**, sér. II, 1305-1308.
- GERSTNER, M. R. (1987): *A Fluid Inclusion and Petrologic Study of the MacTung Scheelite Skarn Deposit, Yukon - Northwest Territories, Canada*. M.S. thesis, Univ. of Utah, Salt Lake City, Utah.
- HANOR, J.S. (1980): Dissolved methane in sedimentary brines: potential effect on the PVT properties of fluid inclusions. *Econ. Geol.* **75**, 603-617.
- HARRIS, F.R. (1977): Geology of the MacMillan tungsten deposit. In 1976 Yukon Mineral Industry Report, Open-file ed., (May, 1977) Dep. Indian Northern Affairs, 20-32.
- HEDENQUIST, J.W. & HENLEY, R.W. (1985): The importance of CO₂ on freezing point measurements of fluid inclusions: evidence from active geothermal systems and implications for epithermal ore deposition. *Econ. Geol.* **80**, 1379-1406.
- HEYEN, G., RAMBOZ, C. & DUBESSY, J. (1982): Simulation des équilibres de phases dans le système CO₂-CH₄ en dessous de 50°C et de 100 bars. Applications aux inclusions fluides. *C.R. Acad. Sci. Paris* **294**, série II, 203-206.
- HOLDAWAY, M.J. (1971): Stability of andalusite and the aluminum silicate phase diagram. *Am. J. Sci.* **271**, 97-131.
- HOLLISTER, L.S. & BURRUSS, R.C. (1976): Phase equilibria in fluid inclusions from the Khtada Lake metamorphic complex. *Geochim. Cosmochim. Acta* **40**, 163-175.
- JACOBS, G. K. & KERRICK, D. M. (1981): Methane: an equation of state with application to the ternary system H₂O-CO₂-CH₄. *Geochim. Cosmochim. Acta* **45**, 607-614.
- KEMP, W.M. (1985): *A Stable Isotope and Fluid Inclusion Study of the Contact Al(Fe)-Ca-Mg-Si Skarns in the Alta Stock Aureole, Alta, Utah*. M.S. thesis, Univ. of Utah, Salt Lake City, Utah.
- KERRICK, D.M. (1972): Experimental determination of muscovite + quartz stability with $P_{(H_2O)} < P_{(total)}$. *Am. J. Sci.* **272**, 946-958.
- _____ & JACOB, G.K. (1981): A modified Redlich-Kwong equation for H₂O, CO₂ and H₂O-CO₂ mixtures at elevated pressures and temperatures. *Am. J. Sci.* **281**, 735-767.
- KRADER, T. & FRANCK, E.U. (1986): Phase equilibria and critical phenomena of the ternary system H₂O-CH₄-NaCl to 500°C and 2500 bar. *Physica* **139-140**, 66-69.
- MARSHALL, D.R., SAITO, S. & KOBAYASHI, R. (1964): Hydrates at high pressures. I. Methane-water, argon-water, and nitrogen-water systems. *Am. Inst. Chem. Eng. J.* **10**, 202-205.
- MATHIESON, G.A. & CLARK, A.H. (1984): The Can-Tung E zone scheelite skarn ore body, Tungsten, Northwest Territories: a revised genetic model. *Econ. Geol.* **79**, 883-901.
- MAY, A.D., STRYLAND, J.C. & WELSH, H.L. (1959): Raman spectra of H₂O and CH₄ at high pressure. *J. Chem. Phys.* **30**, 1099-1100.
- MEINERT, L.D. & HAWKSWORTH, M.A. (1983): Fluid inclusion composition and temperature evolution in a zoned skarn system, Groundhog mine, New Mexico. *Geol. Soc. Am., Abstr. Programs* **15**, 642.
- MILLER, S.L. (1985): Clathrate hydrates in the solar system. In *Ices in the Solar System* (C.J. Klinger, D. Benest, A. Dollfus & R. Smoluchowski, eds.). *NATO Adv. Study Inst. Ser.* **156**, 59-79.
- MULLIS, J. (1979): The system methane-water as a geologic thermometer and barometer from the external part of the Central Alps. *Bull. Minéral.* **102**, 526-536.

- NEWBERRY, R.J. (1982): Tungsten-bearing skarns of the Sierra Nevada. I. The Pine Creek Mine, California. *Econ. Geol.* **77**, 823-844.
- NOAKER, L.J. & KATZ, D.L. (1954): Gas hydrates of hydrogen sulfide-methane mixtures. *Pet. Trans., AIME* **201**, 237-239.
- PARRY, W.T. (1986): Estimation of X_{CO_2} , P, and fluid inclusion volume from fluid inclusion temperature measurements in the system NaCl-CO₂-H₂O. *Econ. Geol.* **81**, 1009-1013.
- PASTERIS, J.D., KUEHN, C.A. & BODNAR, R.J. (1986): Applications of the laser Raman microprobe RAMANOR U-1000 to hydrothermal ore deposits: Carlin as an example. *Econ. Geol.* **81**, 915-930.
- ____ & WOPENKA, B. (1987): Use of the laser Raman microprobe to trace geological reactions. In *Microbeam Analysis* (R.H. Geiss, ed.). San Francisco Press, San Francisco, California (205-209).
- ____, ____ & SEITZ, J.C. (1988): Practical aspects of quantitative laser Raman microprobe spectroscopy for the study of fluid inclusions. *Geochim. Cosmochim. Acta* **52**, 979-988.
- POTTER, R.W., II & BROWN, D.L. (1977): The volumetric properties of aqueous sodium chloride solutions from 0 to 500°C and pressures up to 2000 bars based on a regression of available data in the literature. *U.S. Geol. Surv. Bull.* **1421-C**, 1-36.
- ____, CLYNNE, M.A. & BROWN, D.L. (1978): Freezing point depression of aqueous sodium chloride solutions. *Econ. Geol.* **73**, 284-285.
- RAMBOZ, C., SCHNAPPER, D. & DUBESSY, J. (1985): The P-V-T-X-f(O₂) evolution of H₂O-CO₂-CH₄-bearing fluid in a wolframite vein: reconstruction from fluid inclusion studies. *Geochim. Cosmochim. Acta* **49**, 205-219.
- ROEDDER, E. (1984): The origin of inclusions. In *Fluid Inclusions* (E. Roedder, ed.), *Mineral. Soc. Am., Rev. Mineral.* **12**, 11-46.
- ROO, J.L. DE, PETERS, C.J., LICHTENTHALER, R.N. & DIEPEN, G.A.M. (1983): Occurrence of methane hydrate in saturated and unsaturated solutions of sodium chloride and water in dependence of temperature and pressure. *Am. Inst. Chem. Eng. J.* **29**, 651-657.
- SEITZ, J.C., PASTERIS, J.D. & WOPENKA, B. (1987): Characterization of CO₂-CH₄-H₂O fluid inclusions by microthermometry and laser Raman microprobe spectroscopy: inferences for clathrate and fluid equilibria. *Geochim. Cosmochim. Acta* **51**, 1651-1664.
- SHELTON, K.L. (1983): Composition and origin of ore-forming fluids in a carbonate-hosted porphyry copper and skarn deposit: a fluid inclusion and stable isotope study of Mines Gaspe, Quebec. *Econ. Geol.* **78**, 387-421.
- TURNER, D.R. (1985): *A Petrologic and Fluid Inclusion Study of the Sphalerite Skarns at the Empire Mine, Hanover, New Mexico*. M.S. Thesis, Univ. of Utah, Salt Lake City, Utah.
- VON STACKELBERG, M. & MULLER, H.R. (1954): Feste Gashydrate. II. Struktur und Raumchemie. *Z. Elektrochemie* **58**, 25-39.
- WOPENKA, B. & PASTERIS, J.D. (1986): Limitations to quantitative analysis of fluid inclusions in geologic samples by laser Raman microprobe spectroscopy. *Appl. Spectros.* **40**, 144-151.
- ____ & ____ (1987): Raman intensities and detection limits of geochemically relevant gas mixtures for a laser Raman microprobe. *Anal. Chem.* **59**, 2165-2170.

Received March 30, 1988, revised manuscript accepted August 22, 1989.